Princeton Plasma Physics Laboratory

PPPL-

PPPL
PRINCETON PLASMA
PHYSICS LABORATORY

Princeton Plasma Physics Laboratory
Report Disclaimers

PPPL Report Availability

Princeton Plasma Physics Laboratory:

http://www.pppl.gov/techreports.cfm

Office of Scientific and Technical Information (OSTI):

http://www.osti.gov/bridge

Related Links:

U.S. Department of Energy

Office of Scientific and Technical Information

Fusion Links

Nonlocal transport in the Reversed Field Pinch

G. Spizzo,[1, *] R. B. White,[2] S. Cappello,[1] and L. Marrelli[1]

[1]*Consorzio RFX, Euratom-ENEA Association,*

Corso Stati Uniti, 4 35127 Padova - Italy

[2]*Plasma Physics Laboratory, Princeton University,*

P.O.Box 451, Princeton, New Jersey 08543

(Dated: August 28, 2009)

Abstract

Several heuristic models for nonlocal transport in plasmas have been developed, but they have had a limited possibility of detailed comparision with experimental data. Nonlocal aspects introduced by the existence of a known spectrum of relatively stable saturated tearing modes in a low current reversed field pinch offers a unique possibility for such a study. A numerical modelling of the magnetic structure and associated particle transport is carried out for the reversed-field pinch experiment at the Consorzio RFX, Padova, Italy. A reproduction of the tearing mode spectrum with a guiding center code[1] reliably reproduces the observed soft X-ray tomography. Following particle trajectories in the stochastic magnetic field shows the transport across the unperturbed flux surfaces to be due to a spectrum of Lévy flights, with the details of the spectrum position dependent. The resulting transport is subdiffusive, and cannot be described by Rechester-Rosenbluth diffusion, which depends on a random phase approximation. If one attempts to fit the local transport phenomenologically, the subdiffusion can be fit with a combination of diffusion and inward pinch[2]. It is found that whereas passing particles explore the stochastic field and hence participate in Lévy flights, the trapped particles experience normal neoclassical diffusion.

A two fluid nonlocal Montroll equation is used to model this transport, with a Lévy flight defined as the motion of an ion during the period that the pitch has one sign. The necessary input to the Montroll equation consists of a time distribution for the Lévy flights, given by the pitch angle scattering operator, and a distribution of the flight distances, determined numerically using a guiding center code. Results are compared to experiment. The relation of this formulation to fractional kinetics is also described.

1) R. B. White and M. S. Chance, Phys Fluids 27, 2455 (1984)

2) G. Spizzo, R. B. White, S. Cappello, Physics of Plasmas 14, 102310 (2007)

PACS numbers: 52.20.Dq,52.65.Cc

---

*Electronic address: `gianluca.spizzo@igi.cnr.it`

I. INTRODUCTION

Several heuristic models for non-diffusive transport in plasmas have been developed in order to understand anomalous transport in tokamaks[1–3]. There has been limited possibility of detailed comparision of these models with experimental data, because of scant diagnostic information concerning the nature of the turbulence, and of its often rapid time dependence. Any diffusion process is determined by a sequence of small random steps dx, having a distribution with a mean square step size. Typically the distribution of steps is Gaussian. Nonlocal transport is instead characterized by having a distribution of steps with a long tail, such that a mean square step size does not exist.

For purposes of thermonuclear fusion, the reversed field pinch (RFP)[4, 5] is of interest particularly because of the existence of single helicity states [6, 7], which offer good confinement (for a recent review of the results on single helicity see [8]). However at low current the normal state of the RFP is the multi-helicity state, dominated by a known but large spectrum of relatively stable saturated tearing modes. In this state the reversed field pinch offers a unique possibility for a study of nonlocal transport. The magnetic field in the multihelicity state in a reversed field pinch is typically chaotic but not far above stochastic threshold, so we will see that Rechester-Rosenbluth diffusion is not operative. Large scale coherent structures and streamers exist in the field structure. The situation is analogous to other systems that display nonlocal transport, where large scale streamers or avalanches exist.

Particle transport in toroidal configurations is usually described by splitting the particle flux into a diffusive and a pinch term:

$$\Gamma = -D\nabla n + v \cdot n, \tag{1}$$

where D and v are fit to observed transport in tokamaks [9–12] and reversed-field pinches (RFP) [13–15]. By making a detailed study of ion transport in the RFX we have found a link between pinch velocity and a magnetic chaotic topology[16]. In a chaotic magnetic field near stochastic threshold particle transport is not diffusive.

The low current state in the RFX is characterized by a significant spectrum of magnetic perturbations, which produce a chaotic core in the plasma domain [17]. For this reason,
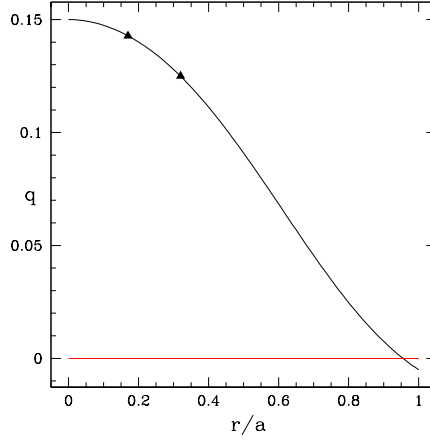
3

FIG. 1: RFX q profile vs minor radius, showing also the $q = 1/7$ and $q = 1/8$ resonances

traditionally a paradigm for transport was based on the assumption of particle diffusion in a stochastic magnetic field, derived by Rechester and Rosenbluth (RR)[18]. In that framework, a field line diffusivity is defined in a random walk approach as $D_{\text{st}} = \langle (\Delta r)^2 / (2L) \rangle$, where brackets $\langle \ldots \rangle$ indicate a mean over a statistical ensemble, typically by averaging over an equilibrium flux surface, and L denotes the distance followed along the field lines. This stochastic field diffusivity is related to the total fluctuation amplitude through $D_{\text{st}} = \left(\tilde{b}/B \right)^2 L_{\text{corr}}$ where L_{corr} is the (parallel) correlation length of the magnetic field lines, $\tilde{b}$ is the perturbation and B is the equilibrium field. D_{st} can also be related to the collisional particle diffusivity through $D_{RR} = D_{\text{st}} \cdot L/\tau$. Typically, the length L travelled in the parallel direction is proportional to the average collision time through the thermal velocity v_{th}, so knowing the stochastic diffusion coefficient one obtains an estimate of the particle diffusivity $D_{RR} = \left(\tilde{b}/B \right)^2 L_{\text{corr}} \, v_{th}$. This traditional picture is however not applicable to the field existing in the RFX, which is chaotic, but not far enough above stochastic threshold to warrant the use of the random phase approximation in calculating transport.

In the multihelicity RFX state the transport has two components, those particles with velocity nearly parallel to the magnetic field (i.e. with pitch $\lambda = v_{\parallel}/v$ close to ± 1) move radially in a subdiffusive manner, ($r^2 \sim t^p$ with $p < 1$) while particles with small pitch diffuse collisionally through the magnetic field. The transport is dominated by the subdiffusive component, and attempting to fit the density profiles to Eq. (1) leads to a large pinch term. The pinch term is thus not a result of particle motion opposite to the density gradient, but a consequence of the non diffusive character of the transport.
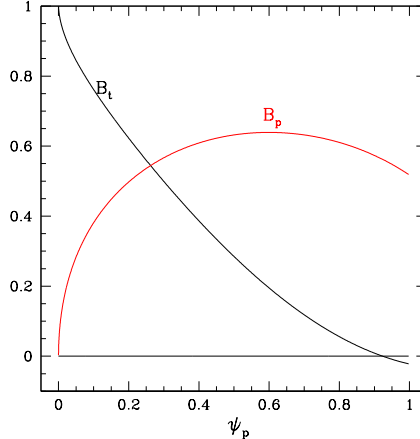
4

FIG. 2: RFX equilibrium field vs minor radius.

The rest of this paper is organized as follows. In section II we discuss the numerical codes used to characterize the transport. The results of the simulations are discussed in section III. Steady state density solutions are found using fixed sources and sinks, the resulting particle flux can be phenomenologically fit with diffusion plus an inward pinch. Also, the time dependence of an initial distribution of particles initiated on a single flux surface is examined. This study reveals the existence of Lévy flights and subdiffusive transport, the distribution of particle steps across the equilibrium flux surfaces has a long tail, and the mean is given only by the system size. Probability distributions of flights across the equilibrium flux surfaces are obtained numerically.

In section IV a nonlocal two fluid Montroll-Weiss model[19, 20] equation is constructed, using the Lévy flight statistics obtained with the guiding center simulations, giving a reasonable description of the essential physics. In section V we discuss the relation of this formalism to fractional kinetics. In section VI are the conclusions.

II. SIMULATIONS

The 3D magnetohydrodynamic (MHD) nonlinear, visco-resistive cylindrical code SpeCyl [17, 21] computes the magnetic field (equilibrium and perturbations) of a chaotic, conventional multiple helicity RFP state with major/minor radii $R/a = 2\text{m}/0.5\text{m} = 4$, Lundquist $S = 3 \times 10^4$, Prandtl number $P = 20$ and pinch parameter $\Theta = B_\theta(a)/\langle B_\phi \rangle = 1.6$. Numerical simulations of magnetic field lines in the stochastic field as well as particle trajectories
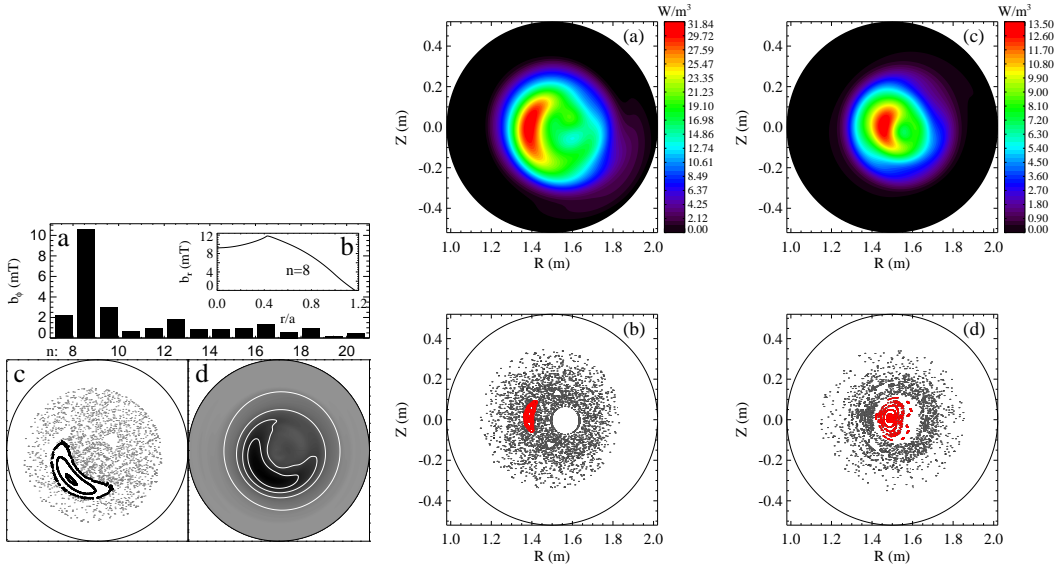
FIG. 3: Comparison of soft X-ray and Poincaré for single helicity states. Taken from [26] and [27].

corresponding to the SpeCyl output are carried out with the code ORBIT, which uses a Runge-Kutta implementation of Hamiltonian guiding center equations in toroidal geometry. This formalism is documented in several publications[22, 23]. In the version of the code for the RFP used here, test particle collisions are implemented through a pitch angle scattering operator and also a classical collision operator, since the banana orbits can be very narrow compared to the gyroradius.

Pitch angle scattering is performed numerically with a Lorentz collision operator, with the pitch defined as $\lambda = v_\parallel/v$, time step dt, and collision frequency ν, through[24]

$$\lambda' = \lambda(1 - \nu dt) \pm \sqrt{(1 - \lambda^2)\nu dt}. \tag{2}$$

SpeCyl simulations mimic a typical low-current discharge of the RFX device [25], with aspect ratio $R_0/a = 4$. The equilibrium q (field helicity) profile and magnetic field components for a typical RFX discharge are shown in Fig2. 1,2. The equilibrium field helicity profile has the range $.15 > q > -.03$. In Fig. 3 are shown comparisons of soft X-ray tomography with Poincaré plots [26, 27] obtained by using the mode spectrum for single helicity states and solving the Newcomb's equations in toroidal geometry [28], using the experimental Mirnov
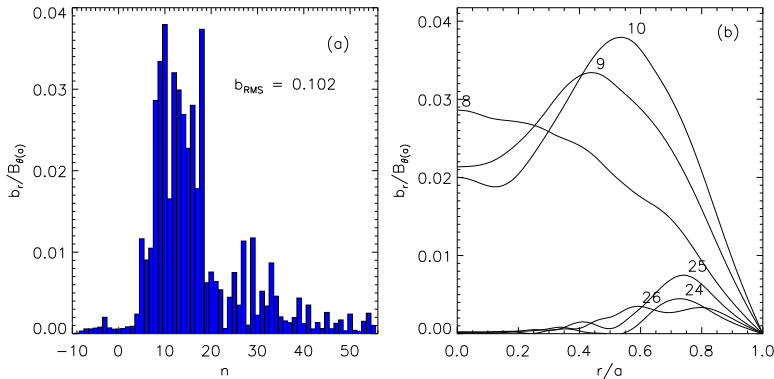
6

FIG. 4: Multi mode state spectrum

data $\delta B(\psi_p, \theta, \phi) = \sum_{m,n} B_{m,n}(\psi_p) sin(m\theta - n\phi)$, $m = 1$, $1 < n < 24$. Fig. 4 shows the typical magnetic spectrum [Fig. 4(a)] and radial profile of $\delta B(r)$ [Fig. 4(b)] for the Multiple Helicity State described by SpeCyl: in this case the spectrum is given in more detail, with $-10 < n < 54$. This state exhibits large scale chaos with no large islands in the RFP core, and the Chirikov stochasticity parameter, a measure of the overlap of nearby magnetic islands, is $C \simeq 5$.

In Fig. 5 is shown the Poincaré plot for the field in the multi-helicity state, showing large scale chaos over most of the plasma. Note that there is no chaos near the axis or near the edge, good flux surfaces prevent field lines in the center of the plasma from reaching either the edge or the magnetic axis. A chain of seven islands is seen near the magnetic axis, corresponding to the smallest n value resonant with this q profile, see Fig. 1. However, there still exist large scale structures and correlations, which can be seen in the plot of Fig. 5 on the right, obtained by following field lines only until they reach $r/a = 0.7$. In this manner the points do not fill the whole plasma volume, and they show the internal structure remaining in the field. Clearly seen is a large $n = 8$ structure, with excursions reaching almost across the whole plasma. This can also be understood from the q profile, shown in Fig. 1. Starting from the magnetic axis, the $n = 8$, $q = 0.125$ island chain is the first unstable island chain. In Fig. 5 one notes that the chaotic domain for small r has eight bumps extending toward the stable $n = 7$, $q = 0.1428$ island chain.

The field characteristics are shown in Fig. 6. We show the determination of the parallel correlation length, defined by following field lines and examining $< r^2 >$. The parallel correlation length $L_{\parallel}$ is defined by the distance along the field at which $(d/dr) < r^2 >$ first
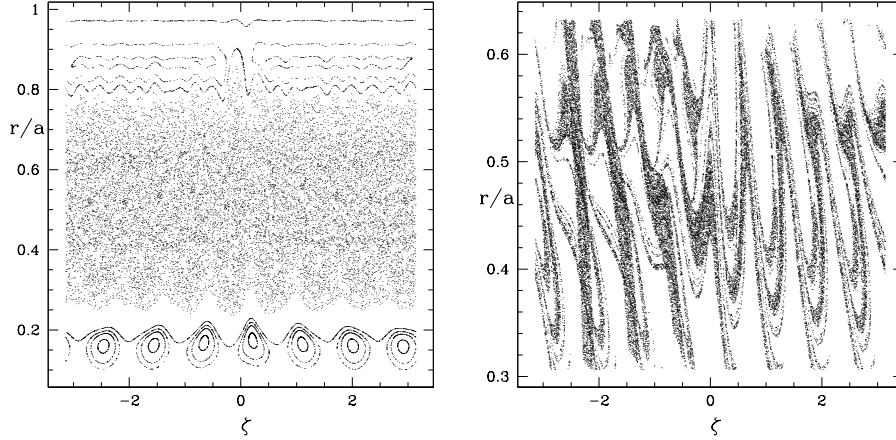
7

FIG. 5: Poincaré plots of the magnetic field
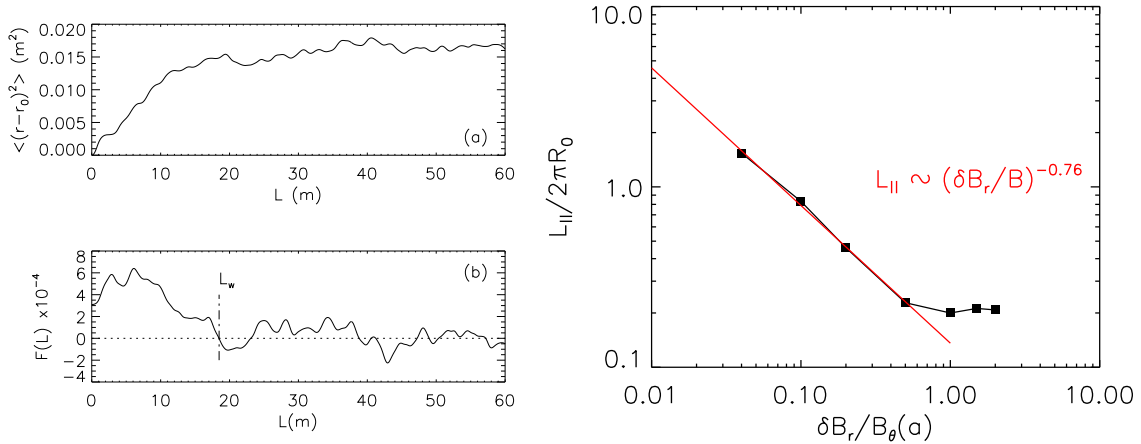

FIG. 6: Magnetic field correlation length $L_\parallel$, and its dependence on the perturbation amplitude.

reaches zero. We show a typical determination of $L_\parallel$, and its dependence on the perturbation magnitude, fit numerically with $(\delta B_r/B)^{-0.76}$. Here and in the following, dependence on perturbation amplitude is normally performed by uniformly increasing all harmonics in the perturbation spectrum, but we also examine the dependence of the transport on the mode spectrum. The typical value of $L_\parallel$ for $\delta B_r/B \simeq 4\%$ (experimental level of fluctuations) is about one toroidal turn.

For field line transport in frozen magnetic turbulence (which is the case of the RFP, for the low-frequency MHD tearing modes usually possess a high degree of spatio-temporal coherence) the Kubo Number is defined as $K = \tilde{b}/B_\theta(a) \times \lambda_\parallel/\lambda_\perp$, and it is shown in Fig. 7. It is equal to 1.5 for the perturbation amplitudes existing in the RFX. Here $\lambda_\parallel = L_\parallel$ and we approximate $\lambda_\perp = a$. This magnitude places the field in the percolation scaling
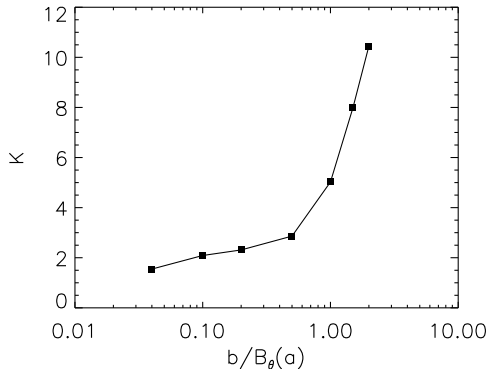
8

FIG. 7: Kubo number versus perturbation amplitude.

regime: this means that field lines spiral around for some time in highly correlated areas, such as the structures evident in Fig. 5, i.e. they are trapped [29]. As a result of the combination of long parallel correlation length and relatively low fluctuation amplitude, one can expect a strong departure from the quasilinear determination of field line diffusivity, and this departure depends on the fluctuation spectrum that determines the structures in Fig. 5 described above. Percolative regimes are found also in simulations of astrophysical magnetic turbulence, as shown by Zimbardo, Veltri and Pommois [30], although they report anomalous transport only when $K \ll 1$.

III. NUMERICAL RESULTS

To examine the transport, we simulate ions at RFX bulk energy (250 eV at plasma current $I_P = 600$ kA and average toroidal field $\langle B_\phi \rangle = 0.2$ T) and density ($n_i = 4 \times 10^{19} \mathrm{m}^{-3}$); modes with poloidal mode number $m = 1$ and toroidal number n up to 26 are considered. Particles are followed using the guiding center code, and subjected to pitch angle as well as classical scattering. As the pitch diffuses due to the collision operator, particles move between poloidally trapped and passing states. Passing particles explore the stochastic field to some distance and participate in long flights along the field line while the chaotic field induces motion across the equilibrium flux surfaces, whereas trapped particles are insensitive to field line chaos. In a fully stochastic field we would expect Rechester- Rosenbluth diffusion across the equilibrium flux surfaces for the passing particles.

We perform two types of simulation. By depositing particles at a particular flux surface ψ_0 and redepositing them when they leave a small annular domain centered about this

9

surface we obtain steady state local density distributions, with a measured rate of flow of particles across flux surfaces through the system. This then results in a local transport rate.

The second method consists of depositing a number of particles at a particular flux surface and collecting time history averages for the evolution of the distribution. Mean values of the square distance from the initial surface versus time as well as statistics regarding motion across equilibrium flux surfaces are recorded.

A. Steady state distributions

The steady state solution to Eq. 1 with source at $x = 0$ and sink at $x = \pm\Delta/2$, and with D, v constant, is symmetric in x and given for $x > 0$ by

$$ n = \frac{\Gamma}{v} \left[1 - e^{\frac{v}{D}(x-\Delta/2)} \right], \tag{3} $$

and shown in Fig. 8. In the limit of $v \to 0$ we have the triangular shape $n = \frac{\Gamma}{D}\left(\frac{\Delta}{2} - x\right)$. For this distribution the density gradient is simply given by the inverse of the domain size, it is not related to the actual equilibrium density gradient.

The evaluation of the local radial transport of particles at some point of the plasma is performed by initially loading ORBIT with a Monte Carlo particle distribution uniform in poloidal (θ) and toroidal (ϕ) angles, and with a triangular density profile radially, centered at r_0 (flux ψ_0) and bounded in minor radius by r_1 and r_2 (flux ψ_1 and ψ_2) so that its width $\Delta = r_2 - r_1$ is large compared to banana width and gyro radius. A triangular profile is the natural steady state distribution for diffusive motion given a source at ψ_0 and sinks at ψ_1 and ψ_2. In the simulation particles exiting the domain are reinserted at ψ_0 with random λ, θ, ϕ. The run time is chosen long enough to allow all particles to perform several cycles through the domain, leading to a steady state distribution (which is normally reached in our case in $20 \div 40$ toroidal transits).

The domain given by Δ is divided into smaller bins of size δ in order to determine the steady state density profile. Numerically the diffusion constant is given by the number of particles N_δ in the central bin $0 < x < \delta$ and the number of particles that exit the domain Δ during the run

$$ D = \frac{\#\text{particles}}{\text{runtime}} \frac{\Delta}{2} \frac{\delta}{N_\delta}. \tag{4} $$
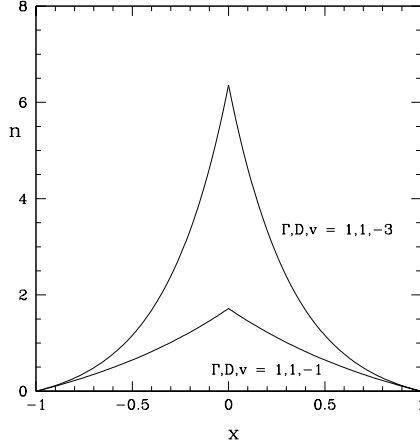
FIG. 8: Theory, diffusion plus pinch steady state

This value is independent of the domain size provided the particle step distance is much smaller than the domain.

An example of an ORBIT run performed in the absence of magnetic chaos is shown in Fig. 9 (solid black lines). The collision frequency is that typical of RFX ($\nu\tau_{\text{tor}} = 0.4$, where τ_{tor} is the collisionless on-axis toroidal transit time), $\Delta = 2.5$ mm, and the ion energy is chosen low ($E = 2.5$ eV), so that the domain can be made small. At higher energies the domain, which must be large compared to the ion cyclotron radius, is large enough so that toroidal effects produce significant asymmetry in the triangular density profile since D in Eq. 1 is no longer constant, but a function of x, complicating the solution, Eq. 3. As expected, the density of particles is within statistical error a triangle [solid line in Fig. 9(a)], the pitch distribution in the domain is uniform [Fig. 9(b)], with $\langle\lambda^2\rangle = \lambda_0^2 = 1/3$. The pitch distribution of particles that exit the domain is also uniform [Fig. 9(c)]. With no perturbations, the field consists of nested magnetic flux surfaces and the neoclassical diffusion D is independent of the size of the domain. Steady state simulations show uniform pitch distribution and approximately triangular $n(\psi)$, with toroidal effects producing some asymmetry. We obtain $D = \Gamma/n(0)\,\Delta/2$, which gives a value $D = 4.2\cdot10^{-5}$ m^2/s close to the neoclassical estimate $D = 1/2\,\nu\rho^2 = 3.8\cdot10^{-5}$ m^2/s (for ion energy of 2.5 eV, $\rho = 0.3$ mm).

Now, let us analyze a case with magnetic fluctuations. Results are shown in Fig. 9 (red dash-dot lines): particle density is shown in frame (a), the distribution of pitch as a function of ψ is shown in (b), and the pitch distribution of lost particles is shown in (c). We observe a significant deviation of the density profile from a triangle, similar to that obtained from the
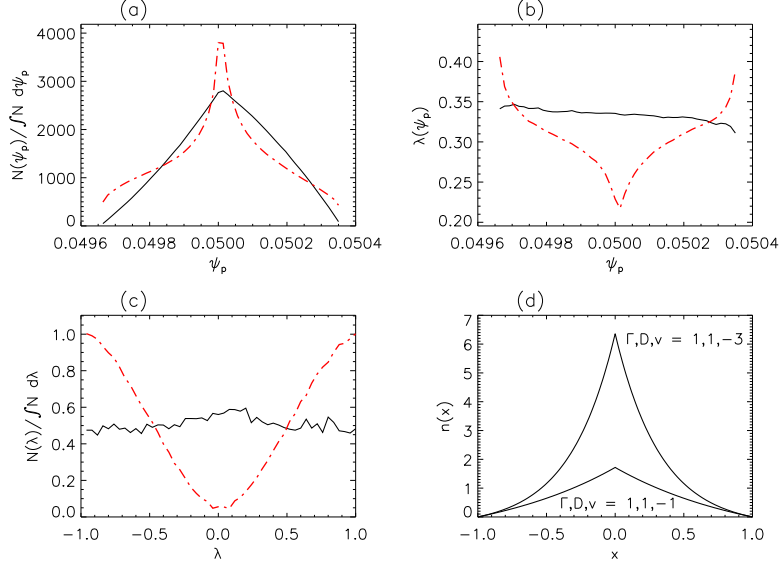
FIG. 9: (Color online). Equilibrium distributions in the unperturbed (——) and chaotic (-.-.-) case: (a) particle density as a function of ψ; (b) distribution in magnitude of pitch $|\lambda|$; (c) density of particles that exit the domain, as a function of the pitch. As a reference, in (d) $n(x)$, $x = r - r_0$, $\Delta/2 = 1$, with pinch, for two different sets of values for particle flux Γ, diffusion coefficient D and pinch velocity $|v|$, is shown. The slight asymmetry of the unperturbed $N(\psi_p)$ distributions about ψ_0 is due to a small magnetic curvature drift effect.

naive pinch model: there is an excess of particles at $\psi = \psi_0$, or rather a depletion of particles at intermediate points between source and sink. Particles at $\psi \simeq \psi_0$ are characterized by lower pitch (in Fig. 9(b) it is evident that without perturbations $\langle \lambda^2(\psi = \psi_0) \rangle < \lambda_0^2 = 1/3$). This means that particles with pitch close to one are rapidly lost: in fact, Fig. 9(c) shows that particles with $\lambda \approx 1$ are more likely to exit the domain. Thus transport can be described in terms of two plasma components, the diffusing trapped particles and the much more rapidly moving passing particles.

The approximate symmetry of $n(r)$ about r_0, is due to the symmetry of the boundary conditions, the slight asymmetry is due to toroidal effects: this means that the pinch velocity is always directed against the density gradient [31]. The difference in transport for particles of different pitch is too rapid for collisions to maintain a uniform pitch distribution. Particles are deposited with uniform pitch, but in the presence of stochastic fields the transport is very pitch dependent, those particles which have pitch nearly ± 1 are quickly lost and thus as they move away from the source the pitch distribution changes, and the transport slows down.

Even though we will find that transport globally is non-diffusive, we can use Eq. (1)
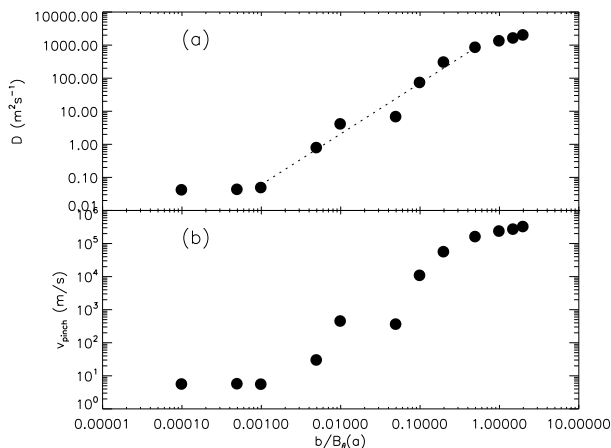
12

FIG. 10: (a) diffusion coefficient D and (b) pinch velocity v as a function of the normalized mode amplitude $\tilde{b}/B_\theta(a)$. D and v are obtained through a least-squares fit of the density distributions $n(\psi)$ inside the triangle. The dashed line in (a) represents a fit of the RR formula.

to match the density profiles, thus obtaining phenomenological transport coefficients. The resulting D for $T_i = 250ev$ is $3.8 \cdot 10^{-5}$ m^2/s for no magnetic field, while $D = 52.6$ m^2/s in the chaotic case. The reference neoclassical D for the chaotic case is $D \approx 0.12$ m^2/s. There is a large pinch of the order $v \sim 6.5 \times 10^3$m/s. Note that if we scale down the amplitudes of the SpeCyl simulation to the experimental $S = 10^6$ [32], we obtain $D \approx 7$ m^2/s and $v \sim 370$m/s. It is straightforward to calculate from Eq.(1) the contribute to the total flux due to diffusion, $\langle \Gamma_D \rangle / \Gamma = \frac{2D}{v\Delta} \left(1 - e^{-v\Delta/2D} \right) \simeq 2.2$, which depends on the product $v\Delta$. Therefore, inward pinch appears in this ad hoc scheme solely to reduce the too large D. In experiments, diffusion is similar ($D \approx 10$m^2/s) and pinch is smaller, $v \sim 15$m/s: notice that in experiments the gradient scale length Δ_{exp} can be larger by one order of magnitude. Experimentally the pinch is large close to the particle sources and directed against the density gradient [13–15], showing a similarity with our simple case. The reduction of magnetic chaos is crucial in reducing D and cancelling the pinch: this happens e.g. in the RFP approaching the single-helicity condition [4, 5, 7].

It is of interest to study the dependence of the phenomenological (D, v) as a function of particle and perturbation parameters. In Table I are shown the results of least-squares fit to the tent distributions for different particle energies and different perturbation amplitude. Results for perturbation amplitude dependence are shown in Fig. 10: D starts from the neoclassical value ($D \sim 0.1$) and then increases as a function of the mode amplitude; v

TABLE I: Results of a least-squares fit of the tent distributions, as a function of the normalized fluctuation amplitude, $\tilde{b}/B_\theta(a)$, and for different ion energies. The last fit is performed at standard energy ($E = 250$ eV), but adding $m = 1$ modes with n up to 50 in the simulations. L_0 is the correlation length, the values of D and v given separately are calculated at the reference $\tilde{b}/B_\theta(a) = 10\%$; $\langle \Gamma_D \rangle / \Gamma$ is the ratio between the diffusive and total flux.

Energy (eV)	L_0 (cm)	D(m²/s)	v (10^3 m/s)	D/v (mm)	$\langle \Gamma_D \rangle / \Gamma$
50	2	50	8	5.8	19
100	1.5	57	9	6.2	15
250^a	1	74	10	6.8	11
500	0.6	93	12	7.4	9
1000	0.4	96	11	8.7	6
250^b	0.9	77	11	6.7	12

^{a}modes $n = 7 - 26$
^{b}modes $n = 7 - 50$

follows more or less the same dependence as a function of $\tilde{b}/B_\theta(a)$, with D/v almost constant when $\tilde{b}$ exceeds a critical value. The ratio D/v (which fixes the ratio $\langle \Gamma_D \rangle / \Gamma$) is nearly independent of ion energy, as shown in Table I for an ion energy range from 50 eV to 1 keV. It is noteworthy that, in the RR framework, according to the derivation of the pinch velocity from the kinetic equations made by Harvey [33], D and v are proportional. This has given support to the application of this formalism to the empirical transport coefficients found in experiments [13–15].

The ratio D/v is also independent of the topology of the magnetic field provided the field is chaotic: this has been checked performing a scan at $E = 250$ eV, but including modes with $m = 1$ and n up to 50 in the ORBIT simulations. Since it depends weakly on particle energy and on the details of the (chaotic) magnetic field (such as the correlation length which will be discussed later), our conclusion is that it depends only on the pitch distribution.

We can also further verify a formal similarity of our simulations with the outcome of the RR formula $D_{RR} = (\tilde{b}/B)^2 L_{\text{corr}} v_{th}$. We can in fact fit the dependence of Fig. 10(a) with a functional form of the type $(\tilde{b}/B)^\beta \cdot L_0 v_{th}$. We obtain $\beta = 1.6$ and $L_0 = 1$ cm. The value of the exponent β is in agreement with that found elsewhere for RFX [34, 35], while L_0, which should coincide with a typical correlation length of the (chaotic) magnetic field lines is smaller by at least one order of magnitude.

We find the correlation length of the magnetic field lines for the case of interest by calculating the spreading $\langle (r - r_0)^2 \rangle$ of field lines initiated at r_0. Following the same procedure
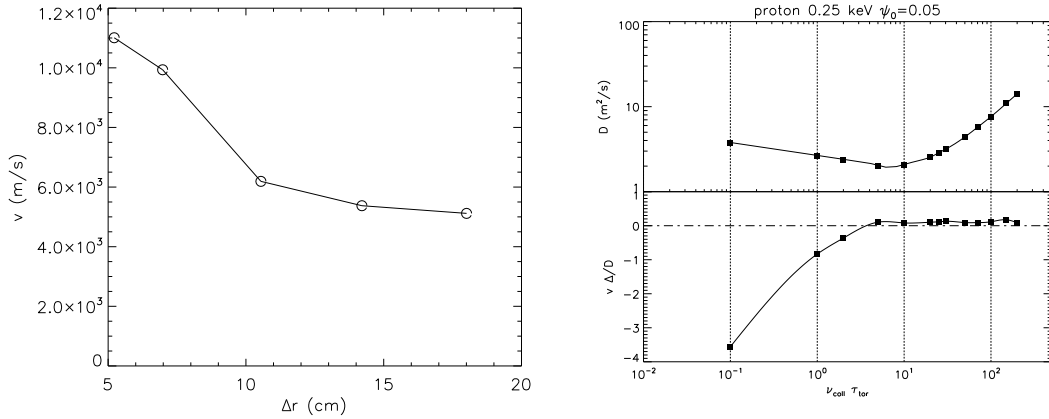
FIG. 11: Scaling of pinch with density scale, and scaling of diffusion and pinch with collision frequency.

highlighted in [34], we find that $L_{\mathrm{corr}} = 10.5$ m, much larger than the correlation length L_0 obtained from our least-squares fit of the D obtained from the triangle distributions ($L_{\mathrm{corr}}/L_0 \simeq 1000$). We interpret this result as due to the fact that only particles with *small pitch* contribute to diffusion in stochastic field lines: particles with $\lambda \approx \pm 1$ contribute to the pinch. This idea is equivalent to assuming that the perpendicular fraction of this thermal velocity contributes to diffusion, $D = D_{\mathrm{st}}\langle v_\perp \rangle$, while the parallel fraction contributes to pinch, $L_0 v = D_{\mathrm{st}}\langle v_\parallel \rangle$, where L_0 is the aforementioned correlation length of the magnetic field re-scaled to the fraction of particles contributing to pinch. The ratio $D/L_0 v$ is therefore independent of the details of magnetic chaos given by D_{st}, and of the particle energy, being roughly:

$$\frac{D}{L_0 v} = \frac{\int v_\perp f(v) d^3 v}{\int |v_\parallel| f(v) d^3 v} = \frac{\int \sqrt{1-\lambda^2} f(\lambda) d\lambda}{\int |\lambda| f(\lambda) d\lambda}. \tag{5}$$

This integral is $\pi/4$ in the case of $f(\lambda) = \lambda^2$, while it is unity when $f(\lambda) = |\lambda|$. The steady state pitch distribution of lost particles gives numerically an intermediate result (0.96), so that, using the value of L_0 for the $E = 250$ eV case of Table I, we obtain a value $D/v = 9.6 \times 10^{-3}$, close to the figure 6×10^{-3} obtained in simulations.

In Fig. 11 is shown the scaling of the pinch velocity with the density scale length and the scaling of the diffusion and pinch velocity with the collision frequency. These scalings are easily understood in terms of the Lévy flights, discussed in the next section.

15

B. Flights

Models for Lévy flight transport in the literature are determined by giving particles a waiting time distribution and a distribution in flight distance. To compare with such models, we define a flight by the sign of the particle pitch. As long as the pitch has one sign, a particle will continue to travel along a magnetic field line, reversing direction with the reversal of the pitch. Thus the flight time is given by the distribution of the Poincaré return times $T_r(t)$ with $\int dt T_r(t) = 1$ for the scattering operator, it is independent of the magnetic field topology, given only by the collision frequency. It is interesting that this operator, although it is diffusive, produces a long time tail in the Poincaré return times, of the form $t^{-1.4}$, easily determined by recording flight times using only Eq. 2. Thus there is no mean time for a flight. A numerically determined distribution is seen in Fig. 12. Times are given in toroidal transit times τ_{tor}, defined as the time for a particle to complete a toroidal transit at the magnetic axis ($\tau_{tor} = 2\pi R_0/v_{th}$). The truncation at $t \simeq 20$ is not a property of the collision operator, it is due to the finite simulation time. Note that for small times, this distribution is determined by the trapped particle bounce time, and has a minimum value given by the deeply trapped bounce time. Although a mean time does not exist, we can define a characteristic time given by

$$T_c^{-1} = \int dt \frac{T_r(t)}{t}.$$ (6)

Since the collision operator from Eq. 2 is a function of νt except in the small dt trapped particle domain, where it is dependent only on the equilibrium field, we expect that $T_c \sim 1/\nu$.

The simulation is performed by launching a large number of passing particles on a particular flux surface r_0, uniformly distributed poloidally and in pitch within the restriction of being passing. They are then followed until the pitch changes sign, defining a flight originating at r_0. For each particle flight, we measure the distance travelled toroidally, the time spent, and the distance moved across flux surfaces. This data allows a determination of the nature of the transport through the exponent p in
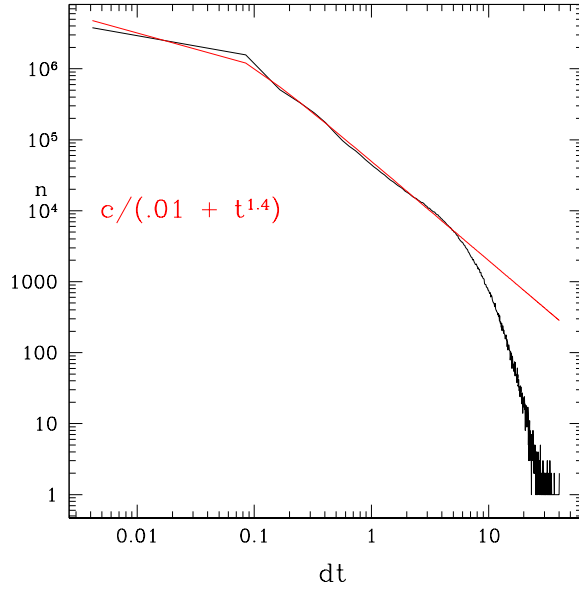
$$< dr^2(t) >= A t^p$$ (7)

16

FIG. 12: Lévy flight distributions in time
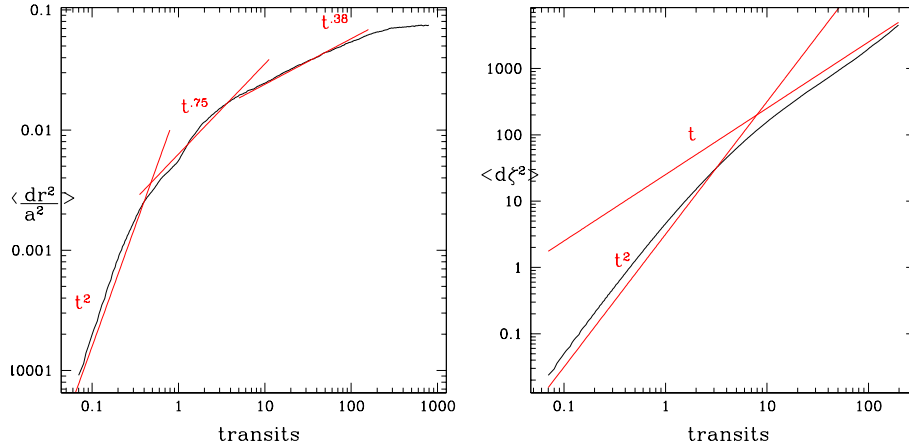

FIG. 13: Time dependence of $< dr^2 >$

as well as the Lévy flight distributions.

Sample results are shown in Fig. 13 and Fig. 14. It is noteworthy that, while in the toroidal angle a ballistic regime is followed at later times by diffusion, in the radial co-ordinate diffusion is *never* reached. Sub-diffusion with $\langle (\Delta r)^2 \rangle \propto t^{0.7}$ is followed by an even stronger subdiffusive regime $\langle (\Delta r)^2 \rangle \propto t^{0.4}$, which is reached corresponding to the diffusive regime in the angular coordinate at about $t = 10$ (in the poloidal angle the behaviour is almost identical). A deeper look at the magnetic topology [see Fig. 14(c)] reveals that in the radial coordinate remnants of magnetic islands act as "sticky" regions for particles,
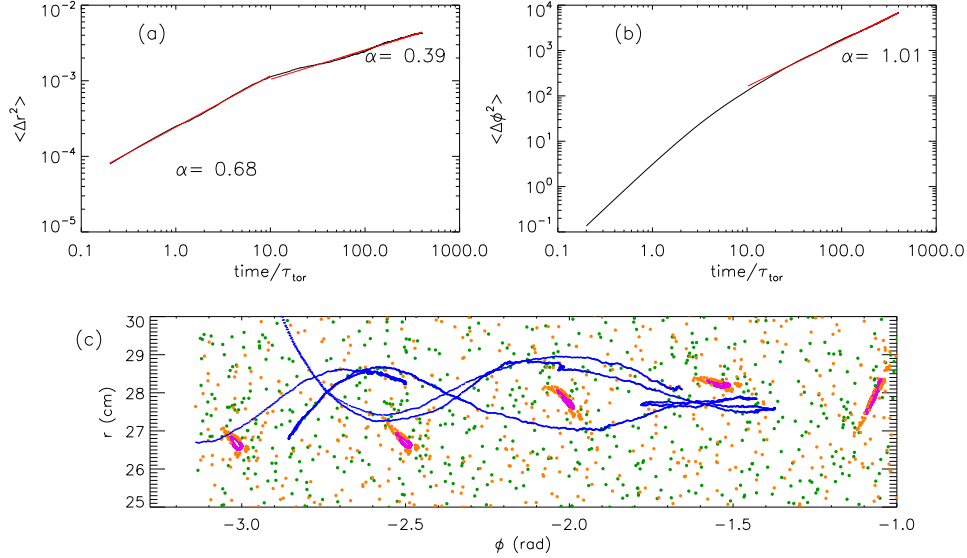
17

FIG. 14: (Color online). Mean square displacements as a function of time (expressed as toroidal transits): (a) radial co-ordinate; (b) toroidal angle. Red line represents a least-squares fit of the form $\langle \Delta r^2 \rangle = C \cdot t^{\alpha}$. Values of α are also reported. (c) Poincaré plot (portion of equatorial cut) of small islands (width $\approx 3 \div 5$ mm) which act as "sticky" regions for particles; in blue a projection on the (r, ϕ) plane of a particle trajectory is overplotted, for $t = 0 \div 10 \, \tau_{\text{tor}}$. $\tau_{\text{tor}} = 2\pi R_0/v_{\text{th}}$ is the (collisionless) transit time.

determining (on average) transport which is slower than the usual RR diffusion, but these islands do not impede motion along the field. This gives an indication that transport is generated by Lévy flights [36, 37] of particles along field lines in the toroidal angle: the same trajectory, meandering in sticky regions radially, generates a more or less slow motion in this coordinate. The presence of two slopes is due to the fact that, at longer timescales, collisions become important in reversing direction along the field, making the toroidal motion diffusive. The radial transport is always subdiffusive, similar to that found in [38]. This analysis confirms early results obtained in RFX concerning field line dynamics [34], and the pioneering theory by Balescu [39]. Similar behavior is seen in the Chirikov-Taylor model [40]. Note that the radial diffusive behavior of the trapped particles (neoclassical banana regime of particles with $\lambda = v_{\parallel}/v \ll 1$ and $\langle (\Delta r)^2 \rangle \propto t^{\alpha}$, $\alpha \approx 1$) is not visible because of its very small magnitude. Untrapped particles cause the mean $(\Delta r)^2$ to reach the boundary of the device long before this term can make an appearance.

In Fig. 15 is shown a sample distribution of flight distances for a monoenergetic particle distribution with energy $250ev$ and collision time of $\nu\tau_{\text{tor}} = 0.4$. At this flux surface the
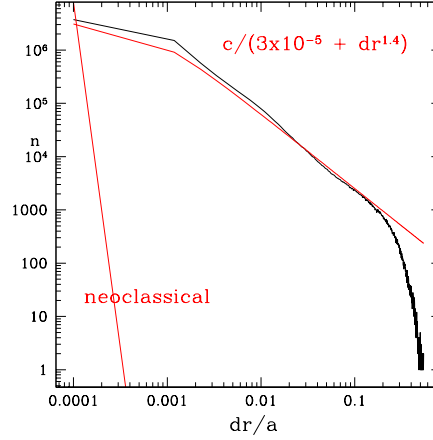
18

FIG. 15: Lévy flight distribution in distance, showing also the equivalant neoclasssical gaussian distribution.

radial distribution also behaves as the -1.4 power for a significant range of distances, similar to the distribution of flight times. This number is not the case in general, the power is found to range from -.8 to -1.6 at different radial locations. But at each radius in the chaotic field, a mean flight distance exists only because of the finite device size, there is no mean radial stepping distance defined by the distribution except through the boundaries.

The scalings seen in Fig. 11 are easily understood in terms of the existence of passing particle Lévy flights. If the density gradient is very steep, passing particle flights easily take particles quickly out of the domain used for the transport determination. The flights thus have a strong effect on the determination of the transport. To produce a small density gradient a much larger domain must be used, and fewer flights are capable of landing outside the domain. Thus the effect of the flights, and hence the pinch velocity, must decrease with the gradient scale length.

The scaling of the diffusion and pinch velocity with collision frequency shown in Fig. 11 is also clear. For very small collisionality the characteristic flight time T_c is very large, flights have a significant range. But $T_c \sim 1/\nu$ and when it is smaller than the time for a particle to go one field correlation length, the flights have no effect on the transport, and the transport becomes diffusive.

19

IV. MODELLING THE TRANSPORT WITH A MONTROLL EQUATION

We now attempt to construct a model for the observed nonlocal transport. Since the trapped and passing particles experience very different behavior, we introduce a two fluid model, with a trapped particle component $n_t(r,t)$ and a passing particle component $n_p(r,t)$. We use averages over flux surfaces and velocity space to obtain this representation of the distribution with only two scalar functions. The passing particles participate in flights, and the trapped particles only diffuse. There is of course collisional transfer between trapped and passing species, depending on the local mean trapped passing boundary. This we determine numerically, and it is shown in Fig. 16.

We thus posit a two component Montroll master equation model given by

$$\partial_t n_t(r,t) = \int_0^t dt' \int_0^1 dr' n_p(r',t') P(r,r',t,t') - \nu a(r) n_t(r,t) + \nu b(r) n_p(r,t) + .5\nu\rho^2(r)\partial_r^2 n_t(r,t),$$

$$\partial_t n_p(r,t) = -\nu b(r) n_p(r,t) + \nu a(r) n_t(r,t) - \int_0^t dt' \int_0^1 dr' n_p(r',t') \int_0^1 dr P(r,r',t,t'). \tag{8}$$

The trapped fraction determining the trapped-passing transfer rates, a and b, the collisional transfer rate ν, and the gyro radius ρ are all position dependent. The propagator $P(r,r',t,t')$ describes the flight statistics. Since at the end of a flight, when the pitch changes sign, a particle is trapped, the flights contribute positively to the trapped particle density at the flight termination point. We also include the neoclassical diffusion term for the trapped species. It is negligible for the passing particles. We have omitted sources or sinks from these equations, which can easily be added. Without a source or sink the total particle number $\int dr[n_p + n_t]$ is conserved.

The flights originating at r',t' and ending at r,t are given by the probability $P(r,r',t,t')$, which must be obtained numerically from guiding center flight statistics. Examples of the propagator $P(r,r',t,t')$ for two values of r' and $t' = 0$ and for $250ev$ and $\nu\tau_{\text{tor}} = 0.4$ are given in Fig. 17. There are several important things to note about these propagators. First, they are not only very position dependent, they are also very asymmetric in flight direction, because of the variation radially of the degree of stochasticity of the field. Second, they in no way can be factored into functions of space and time by $P(r,r',t,t') = f(r,r')g(t,t')$. In particular, this factorization, commonly used in continuous time random walk (CTRW) theories, violates causality. It has also been shown by Zaslavsky that many map models
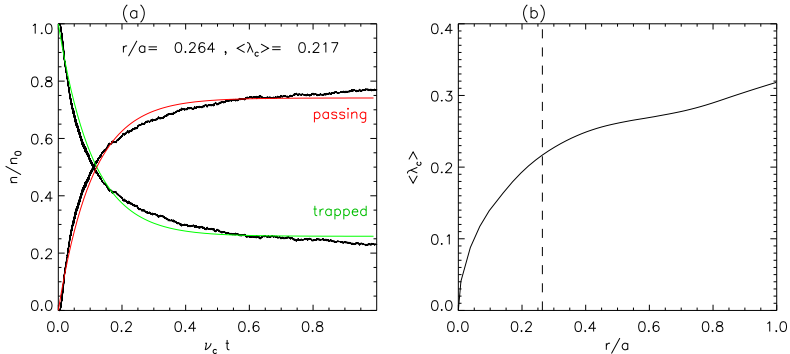
FIG. 16: Trapped passing boundary determination. In (a) is shown a simulation at a particular flux surface, to find the mean trapped and passing populations. In (b) is shown the mean pitch (at the outboard midplane) giving the transition between trapped and passing, versus minor radius.
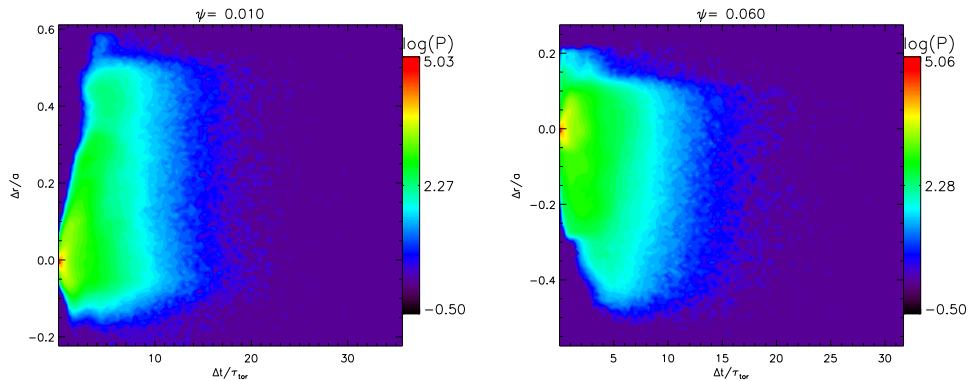

FIG. 17: Propagators shown at initial location $r = .01a$ and $r = .06a$

do not obey factorization [41], as for example the case of advected particles in the 3-vortex flow [42]. Our propagators instead take into account the local properties of the magnetic field as well as the plasma boundaries. They also depend on particle energy and collisionality, and hence plasma density.

Some preliminary simulations have been performed using Eqs. 8. We have looked at simulations of both types of experiments described in section III. A numerical implementation of these equations is fairly rapid, complicated only by the necessity of keeping a time history of information at all relevant radii. Results are shown in Fig. 18, with a confirmation of the $t^{.75}$ behavior in the initial evolution of $< r^2 >$ out to a few toroidal transit times, and the reproduction of the pinch effect in a steady state simulation. Frame (a) shows the steady state trapped and passing populations, and (b) the local trapped fraction.

Once the initial distribution has spread enough so that enough particles are propagating also back toward the initial radius (the toroidal diffusion domain) we expect this simulation
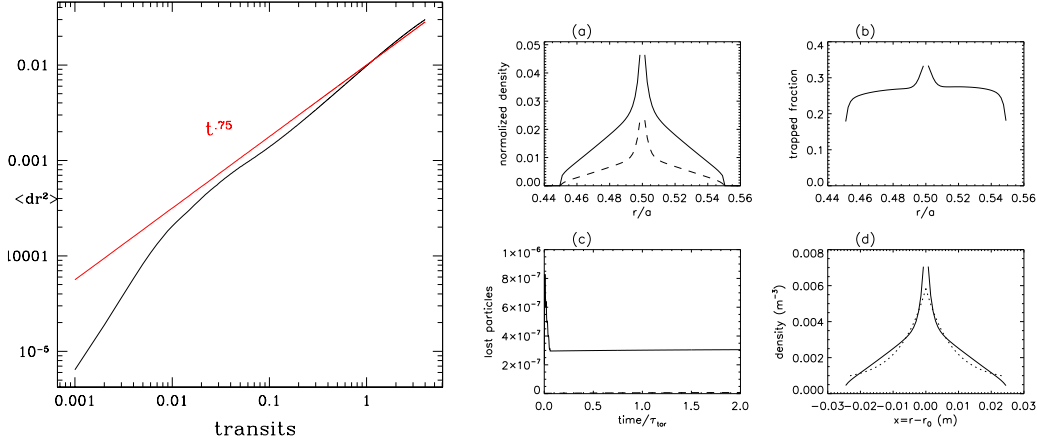
FIG. 18: Subdiffusive behavior and the pinch effect, found using the Montroll equation. The plot of $< dr^2 >$ shows the initial subdiffusive $t^{.75}$ behavior. Plots (a) and (b) show the Montroll equation reproduction of the steady state local solution, giving density profiles for trapped (solid) and passing (dashed) species, and the local trapped fraction.

to reproduce the $< r^2 > \sim t^{.4}$ behavior.

By including source and sink terms, these equations can be used to simulate the complete global steady state density in RFX, and to compare with local determinations of the phenomenological diffusion and pinch values.

V.   FRACTIONAL KINETICS

Zaslavsky[43] and others[1] have championed the use of fractional derivatives for nonlocal transport studies. These models use the Continuous Time Random Walk treatment, and consist of a waiting time distribution, $\psi(t - t')$, and a transition probability $P(r - r')$ for jumping from r' to r. The factorization of the propagator into spatial and time functions permits the useful introduction of Fourier transform techniques. Fractional kinetics is fully determined by the two parameters that describe the space and time asymptotic properties of the stochastic processes. The fractional derivative in space and time results from Lévy processes, The super- or sub-diffusive nature of the transport $< r^2 >= t^p$ is related to the asymptotic behavior of the space and time probability distributions.

The nonlocal transport is described by the generalized diffusion equation, also known as Fractional Kinetic Equation (FKE): $\partial_t f = \chi_a D_x^\alpha f$, where the αth derivative of $f(x)$ is a

nonlocal integro-differential operator

$$_aD_x^\alpha f = \frac{1}{\Gamma(m-\alpha)}\frac{\partial^m}{\partial x^m}\int_a^x \frac{f(y)}{(x-y)^{\alpha+1-m}}dy \tag{9}$$

which is an analytic extension of usual differentiation (α integral) to the real number line, and this combination of differentiation and integration leads to its nonlocality.

But we find numerically that at least for this case the spatial transition probability is a function of the flight time. There is no factorization of $P(r, r', t, t')$ into $P(r, r')\psi(t, t')$ which in any case is non causal. In addition the Green's function $P(r, r', t, t')$ is not translation invariant, the Lévy tail depends on location. Thus to represent our case the fractional derivative α would need to be x dependent, and it is not clear that this formalism makes sense in this case. In addition the bounded domain, easily handled by the Montroll equation, makes treatment using fractional derivatives more complicated. The approach of fractional kinetics appears to be more suitable for treating a homogeneous case, and can offer insight in this limit.

Of course we do not know how to find $P(r, r', t, t')$ or α analytically from the properties of the magnetic field, such as the spectrum, the field correlation length, the Chirikov overlap parameter and the Kubo number, which would be the ultimate goal for predicting transport. A strong motivation for studying this case is that it offers a test bed for the determination of particle transport in a nonlocal system from the properties of the magnetic field turbulence. The greater complexity required by the formalism of the Green's function $P(r, r', t, t')$ or the FKE is balanced by the substantially lower degree of a priori assumptions concerning system properties. In fact, when choosing a simple approach to transport (often through the habit of describing experimental data in terms of usual diffusion/pinch), one should bear in mind the many probabilistic assumptions involved, namely: a Markovian process for waiting times, an isotropic Gaussian distribution of steps, and, last but not least, locality ($dr/a \ll 1$). As reported extensively elsewhere [1, 41] these assumptions often conflict with the real dynamics of the system, requiring more complex tools to describe transport.

VI. CONCLUSION

Ion transport in the multihelicity RFX is subdiffusive, and the transport can be fit phenomonologically with diffusion and an inward pinch. This behavior is similar to that found for turbulent transport across stable sheared zonal flows[44], and may be a general property of systems exhibiting chaos, but not sufficiently above stochastic threshold to permit the use of random phase approximations.

We find that a pinch velocity v appears in the expression of the particle flux in a chaotic field: plasma radial transport is the combination of two different components, neoclassical diffusion due to the trapped particles and subdiffusive Lévy flight transport due to the passing particles, the former arising through toroidal geometry, the latter being an outcome of the chaotic topology of the magnetic field. Passing particles dominate on large scales (see Fig. 14), but trapping is fundamental in determining local features (Fig. 9).

Full scale global simulations using a Montroll equation are possible, giving a realistic steady state description of the density profile, including sources and sinks. The inclusion of trapped and passing species, with collisional transfer between them is essential to reproduce the pinch effect observed with the guiding center simulations. The fact that the propagator in time and space is determined using guiding center simulations in the chaotic field found in RFX means that the local properties of the field and the boundary conditions are properly accounted for. The propagator cannot be factored into time and space functions, it is a complicated causal function, and it reflects the very inhomogeneous field properties as well as the finite plasma boundaries.

EURATOM/ENEA.

---

[1] D. del-Castillo-Negrete, <u>Turbulent Transport in Fusion Plasmas</u> (First ITER International Summer School, AIP Conference Proceedings No 1013 (AIP, Melville NY), p 207, 2008),

[2] B. A. Carreras, D. Newman, V.E. Lynch, P. Diamond, Phys. Plasmas **3**, 8 (1996).

[3] R. O. Dendy, T.K. March, S.C. Chapman, J.A. Merrifield, ECA **28G**, 1.106 (2004).

[4] D. F. Escande, R. Paccagnella, S. Cappello, F. D'Angelo, and C. Marchetto, Phys. Rev. Lett. **85 (15)**, 3169 (2000).

[5] P. Martin et al., Nucl. Fusion **43**, 1855 (2003).

[6] P. Martin, L. Marrelli, A. Alfier, F. Bonomo, D. F. Escande, P. Franz, L. Frassinetti, M. Gobbin, R. Pasqualotto, P. Piovesan, et al., Plasma Phys. Control. Fusion **49**, A177 (2007).

[7] R. Lorenzini, D. Terranova, A. Alfier, P. Innocente, E. Martines, R. Pasqualotto, and P. Zanca, Physical Review Letters **101**, 025005 (pages 4) (2008), URL `http://link.aps.org/abstract/PRL/v101/e025005`.

[8] S. Cappello, D. Bonfiglio, D. F. Escande, S. C. Guo, A. Alfier, and R. Lorenzini (RFX Team), <u>The Reversed Field Pinch toward magnetic order: a genuine self-organization</u> (Joint Varenna-Lausanne International Workshop on Theory of Fusion Plasmas, AIP Conference Proceedings (AIP, Melville NY), 2008), vol. 1069, pp. 27–39, URL `http://link.aip.org/link/APC/1069/27/1`.

[9] B. Coppi and N. Sharky, Nucl. Fusion **21**, 1363 (1981).

[10] C. Angioni et al., Phys. Rev. Lett. **90**, 205003 (2003).

[11] X. Garbet et al., Plasma Phys. Control. Fusion **46**, B557 (2004).

[12] R. W. Harvey, O. Sauter, R. Prater, and P. Nikkola, Phys. Rev. Lett. **88**, 205001 (2002).

[13] L. Carraro et al., Plasma Phys. Control. Fusion **42**, 731 (2000).

[14] R. O'Connell et al., Phys. Rev. Lett. **91**, 045002 (2003).

[15] D. Gregoratto et al., Nucl. Fusion **38**, 1199 (1998).

[16] G. Spizzo and R.B. White and S. Cappello, Phys. Plasmas **14**, 102310 (2007).

[17] S. Cappello, Plasma Phys. Control. Fusion **46**, B313 (2004).

[18] A. B. Rechester and M. N. Rosenbluth, Phys. Rev. Lett. **40**, 38 (1978).

[19] B. Krenke and N. Montroll, J. Stat. Phys **9**, 45 (1973)

[20] B. D. Hughes, M. F. Shlesinger, and E. W. Montroll, Proceedings of the National Academy of Sciences of the United States of America **78**, 3287 (1981), http://www.pnas.org/content/78/6/3287.full.pdf+html, URL `http://www.pnas.org/content/78/6/3287.abstract`.

[21] S.Cappello and D. Biskamp, Nucl. Fusion **36**, 571 (1996).

[22] R. B. White, <u>The theory of toroidally confined plasmas</u> (Imperial College Press, 2006), 2nd ed.

[23] R. B. White, <u>Turbulent Transport in Fusion Plasmas</u> (First ITER International Summer School, AIP Conference Proceedings No 1013 (AIP, Melville NY), pp 59 and 127, 2008),

[24] A. H. Boozer and G. Petravic, Phys. Fluids **24**, 851 (1981).

[25] G. Rostagni, Fusion Engineering and Design **25**, 301 (1995).

[26] I. Predebon, L. Marrelli, R. B. White, and P. Martin, Phys. Rev. Lett. **93**, 145001 (2004).

[27] P. Franz, L. Marrelli, P. Piovesan, I. Predebon, F. Bonomo, L. Frassinetti, P. Martin, G. Spizzo, B. E. Chapman, D. Craig, et al., Physics of Plasmas **13**, 012510 (pages 15) (2006), URL `http://link.aip.org/link/?PHP/13/012510/1`.

[28] M. Gobbin, L. Marrelli, and R. B. White, Plasma Physics and Controlled Fusion **51**, 065010 (14pp) (2009), URL `http://stacks.iop.org/0741-3335/51/065010`.

[29] K. H. Spatschek, <u>Turbulent Transport in Fusion Plasmas</u> (First ITER International Summer School, AIP Conference Proceedings No 1013 (AIP, Melville NY), p 250, 2008),

[30] G. Zimbardo, P. Pommois, and P. Veltri, Physica A: Statistical Mechanics and its Applications **280**, 99 (2000), ISSN 0378-4371, URL `http://www.sciencedirect.com/science/article/B6TVG-404H39H-F/%2/5abd75f747f6545589263b38a096f9e1`; G. Zimbardo, P. Veltri, and P. Pommois, Phys. Rev. E **61**, 1940 (2000).

[31] B. Ph. Van Milligen, B. A. Carreras, and R. Sánchez, Phys. Plasmas **11**, 3787 (2004).

[32] D. Terranova, T. Bolzonella, S. Cappello, P. Innocente, L. Marrelli, and R. Pasqualotto, Plasma Phys. Control. Fusion **42**, 843 (2000).

[33] R. W. Harvey, M. G. McCoy, J. Y. Hsu, and A. A. Mirin, Phys. Rev. Lett. **47**, 102 (1981).

[34] F. D'Angelo and R. Paccagnella, Phys. Plasmas **3**, 2353 (1996).

[35] L. Frassinetti, A. Alfier, R. Pasqualotto, F. Bonomo, and P. Innocente, Nuclear Fusion **48**, 045007 (13pp) (2008), URL `http://stacks.iop.org/0029-5515/48/045007`.

[36] R. Sánchez, B. Ph. Van Milligen, and B. A. Carreras, Phys. Plasmas **12**, 056105 (2005).

[37] B. Ph. Van Milligen, B. A. Carreras, and R. Sánchez, Plasma Phys. Control. Fusion **47**, B743 (2005).

[38] T. Geisel and S. Thomae, Phys. Rev. Lett. **52 (22)**, 1936 (1984).

[39] R. Balescu, Phys. Rev. E **51 (5)**, 4807 (1995).

[40] R. B. White, S. Benkadda, S. Kassibrakis, and G. M. Zaslavsky, Chaos **8 (4)**, 757 (1998).

[41] G. M. Zaslavsky, Hamiltonian Chaos and Fractional Dynamics (Oxford University Press, Great Clarendon Street, Oxford OX2 6DP, 2008), chap. 18, p. 281.

[42] L. Kuznetsov and G. M. Zaslavsky, Phys. Rev. E **61**, 3777 (2000).

[43] G. M. Zaslavsky, Phys. Rep. **371 (6)**, 461 (2002).

[44] J. A. Mier, R. Sánchez, L. García, B. A. Carreras, and D. E. Newman, Physical Review Letters **101**, 165001 (pages 4) (2008), URL http://link.aps.org/abstract/PRL/v101/e165001.